



Dynamic and thermodynamic upper-ocean response to the passage of Bay of Bengal cyclones ‘Phailin’ and ‘Hudhud’: a study using a coupled modelling system

Deepashree Dutta · Balaji Mani ·
Mihir Kumar Dash 

Received: 25 June 2018 / Accepted: 24 July 2019
© Springer Nature Switzerland AG 2019

Abstract Understanding the upper-ocean response to tropical cyclones (TCs) in terms of sea surface temperature (SST) cooling is of prime importance in the prediction of TC intensity. However, the magnitude of cooling during the passage of TC varies depending on storm characteristics and pre-existing upper-ocean conditions such as the presence of ocean eddy and upper-ocean stratification. The present study investigates the upper-ocean response to two post-monsoon Bay of Bengal (BoB) cyclones, Phailin (October 2013) and Hudhud (October 2014), those followed almost a similar track, in association with pre-existing oceanic conditions using a fully coupled ocean-atmosphere modelling system. The spatial structure and temporal evolution of SST cooling induced by the two cyclones and the physical processes governing the cooling are examined. Analysis shows that the intensity of Phailin is significantly reduced when it encountered the regime of lower tropical cyclone heat potential (TCHP) associated

with pre-existing cold core eddy (CCE). Intense upwelling with an average of 0.6 m/h is observed over CCE that resulted in strong temperature tendency of $-4.2\text{ }^{\circ}\text{C}$ prior to landfall. Though average TCHP in the generation region of Hudhud was 50 kJ/cm^2 , the storm drew sufficient energy from the underlying ocean due to its slow translation speed. Presence of shallow thermocline over extended region and weaker upper-ocean stratification enhanced SST cooling over a larger region after passage of the TC Hudhud. Finally, the present study brings in clarity that the upper-ocean condition and the relative position of the mesoscale oceanic features to the storm track are responsible for the intensification of the TC and the recovery of the ocean surface.

Keywords Tropical cyclone · SST cooling · Phailin · Hudhud · Mesoscale eddy

This article is part of the Topical Collection on *Terrestrial and Ocean Dynamics: India Perspective*

Electronic supplementary material The online version of this article (<https://doi.org/10.1007/s10661-019-7704-9>) contains supplementary material, which is available to authorized users.

D. Dutta · B. Mani · M. K. Dash (✉)
Centre for Oceans, Rivers, Atmosphere and Land Sciences, Indian Institute of Technology Kharagpur, Kharagpur 721302, India
e-mail: mihir@coral.iitkgp.ac.in

B. Mani
Willis Towers Watson (WTW) Global Delivery and Solutions
India Private Limited, Mumbai, India

Introduction

The Bay of Bengal is one of the most vulnerable basins to tropical cyclones (TCs). Sea surface temperature (SST) greater than $26.5\text{ }^{\circ}\text{C}$ (Gray 1998) with favourable atmospheric conditions can lead to the generation of TCs in the Bay of Bengal (BoB). It has been long recognised that TCs gain their energy from the ocean surface through sensible and latent heat fluxes (Riehl 1950; Palmen 1948). The low pressure system absorbs energy from the ocean surface and intensifies into a TC in a conducive environment. Further, intensification of TCs is associated with increased evaporation from the ocean surface and strong turbulent mixing

in the oceanic mixed layer, causing surface cooling (Lin et al. 2005; Chan et al. 2001; Bosart et al. 2000). This cooling of the sea surface results in the decrease in enthalpy fluxes which leads to reduction in storm intensity and usually referred to as ocean negative feedback to storm intensification. Thus, sea surface cooling response to TC forcing plays a crucial role in storm intensification process. The sensitivity of storm intensity to sea surface cooling has been demonstrated by numerous observational (Demaria and Kaplan 1994; Elsner et al. 2013), theoretical (Petrova 2010; Emanuel 1986), and numerical model (Tuleya and Kurihara 1982; Chang and Anthes 1979) studies.

Numerical hurricane models consider SST forcing as a lower boundary condition, whereas, numerical ocean models are forced with surface fluxes. In both of the cases, influence of the coupled atmosphere-ocean feedback system is neglected (Davis et al. 2008). Nevertheless, the potential contribution of the spatial extent of SST cooling relative to the eye of the TC has to be taken care of (Yablonsky and Ginis 2009). The axisymmetric coupled models were not able to produce optimum results as they neglected the rightward bias of ocean response with respect to the track of TC. This leads to the extensive use of three-dimensional coupled models in the recent decade (Knaff et al. 2013; Chan et al. 2001; Bender and Ginis 2000). These studies indicate strong impact of storm-induced cooling in weakening TC intensity. Additionally, the presence of oceanic mesoscale features such as eddies, fronts, and rings instigates the cyclone by modulating heat and momentum exchange at the air-sea interface. Evidences have shown that rapid intensification of TCs is often associated with the presence of warm core rings, eddies (Patnaik et al. 2014), loop current, etc. (Sun et al. 2006). Many studies have shown the intensification of hurricanes and typhoons as they pass over the regions having high upper-ocean heat content (Lin et al. 2005; Shay et al. 2000; Shay and Uhlhorn 2008). Contrasting, an increased SST cooling occurs in the presence of pre-existing cold core eddies (Jaimes et al. 2011; Lu et al. 2016; Sun et al. 2014). However, studies on a similar nature, using coupled numerical models, are limited over the BoB.

Relatively high SST (28–30 °C), thermodynamically unstable and weak lower tropospheric wind shears during October–December and April–June favour the development of TC over the BoB (McPhaden et al. 2009). Additionally, availability of high tropical cyclone heat potential (TCHP) ($\sim 58 \text{ kJ/cm}^2$) in the Andaman Sea, central and southern BoB in the post-monsoon season (October–

November), provides a conducive environment for the formation of TCs (Sadhuram et al. 2004). Observational evidences have proven that SST cooling induced by TC is relatively lower during post-monsoon season compared with pre-monsoon and is attributed to the presence of thick barrier layers and existence of subsurface thermal inversions (Neetu et al. 2012). After the passage of TC, SST exhibits prominent spatial and temporal variability. However, the magnitude and spatial extent of SST cooling and its recovery time are dependent on the intensity and the translation speed of the storm (Dare and McBride 2011). A study on Odisha super cyclone shows that interaction of the storm with warm core eddy enhanced its intensity by 260% (Patnaik et al. 2014). Though numerical studies have confirmed the negative feedback of TC-induced SST cooling on intensity as discussed earlier, upper-ocean response in conjunction with pre-existing mesoscale features is rarely investigated using a coupled ocean-atmosphere model, especially for BoB cyclones. Also, lack of in situ observations in the BoB, role of intensity, and size and movement of storm on regional SST cooling have not been studied extensively. The present study investigates the upper-ocean response to TC in association with pre-existing oceanic conditions using a coupled ocean-atmosphere modelling system, hereafter referred to as the mesoscale coupled modelling system (MCMS). MCMS includes the non-hydrostatic atmospheric model (ARW-WRF, Advanced Research Weather Research and Forecasting) and the three-dimensional hydrostatic ocean model (ROMS, Regional Ocean Modelling System). The prime aim of this numerical experiment is to examine the upper-ocean response to two post-monsoon BoB very severe cyclones, Phailin (in the year 2013) and Hudhud (in the year 2014), which followed almost a similar track before landfall.

TC Phailin originated from a remnant of a cyclonic circulation over the north Andaman Sea and appeared as a depression at 00:00 UTC of 8 October centred near (12.0° N, 96.0° E). It moved in northwest direction and intensified into a cyclonic storm by 12:00 UTC of 9 October. By 6:00 UTC of 10 October, it developed into a very severe cyclonic storm. It intensified further and attained its maximum intensity on 11 October around 3:00 UTC, having a wind speed of 115 knots and central sea level pressure of 940 hPa. The storm crossed the east coast of India near Gopalpur, Odisha, around 17:00 UTC of 12 October 2013. The storm track is shown by thick dark lines in Fig. 1c. The black dots on the storm track represent minimum pressure observed at 12 UTC of each

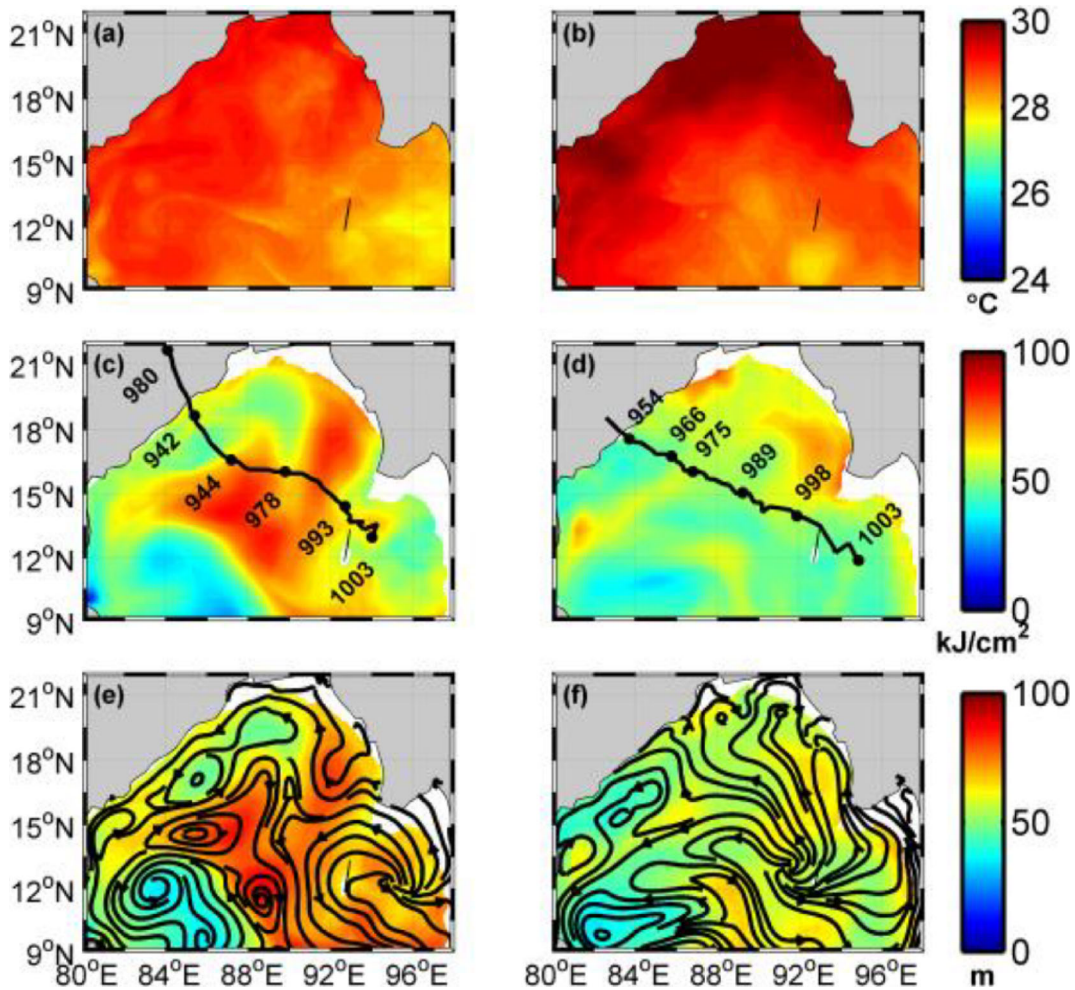


Fig. 1 Pre-storm (a) sea surface temperature (SST), (c) tropical cyclone heat potential (TCHP) and (e) 26 °C isothermal layer depth (shaded) and ocean currents average for upper 100 m (streamlines) for Phailin on 8 October 2013. (b), (d), and (f) are the same as (a), (c), and (e) respectively for Hudhud on 7 October

2014. The thick dark lines on (c) and (d) represent the storm tracks for Phailin and Hudhud respectively. The black dots on the storm track in ‘c’ (‘d’) represent minimum sea level pressure at 12 UTC for Phailin, 8–13 October 2013, (Hudhud, 7–12 October 2014) as one moves from right to left in the figures

day, 8–13 October 2013, as one moves from right to left in the figure.

On the other hand, the TC Hudhud formed as a low pressure system in the Andaman Sea on 6 October 2014. Further, it intensified and took the form of a TC on 10 October. It reached its peak intensity on 11 October 2014 with a minimum central pressure of 950 hPa and average wind speed of 185 km/h. Landfall occurred on 12 October 2014 near Visakhapatnam, India. The track of Hudhud is shown by thick dark lines on Fig. 1d. The black dots on the storm track represent minimum pressure observed at 12 UTC of each day, 7–12 October 2014, as one moves from right to left in the figure. Moreover, Hudhud developed over the same region and followed a similar track as

Phailin before its landfall near Visakhapatnam, Andhra Pradesh, India.

This paper is organised as follows. Model description and datasets are described in detail in the ‘Model description’ section. The ‘Data used’ section presents a comprehensive comparative analysis of the pre-existing physical states of the upper surface of BoB before/during the generation of TC. The ‘Numerical experiments’ section presents thermal and dynamic changes in the upper ocean during TCs Phailin and Hudhud. Upper-ocean recovery aftermath of the storm passage and discussions are presented in the ‘Pre-storm ocean conditions over BoB and intensification of TC’ and ‘Upper-ocean response to TC passage’ sections, respectively. The dynamical responses

of the upper ocean to the TC are presented in the ‘[Dynamical upper-ocean response to the TC](#)’ section; the recovery of the upper surface of the ocean is described in the ‘[Upper-ocean recovery](#)’ section, followed by the summary of the study in the ‘[Summary](#)’ section.

Model description

In this study, simulations of TCs Phailin and Hudhud are carried out using a MCMS and the results are validated with the observations. The evaluation of MCMS for the prediction of BoB cyclones is reported by Mandal et al. (2016). It includes a non-hydrostatic atmosphere model (ARW-WRF) and a three-dimensional hydrostatic ocean model (ROMS). The Model Coupling Toolkit (MCT) is used to couple the two models efficiently. The following sections provide a brief description of these two components of MCMS.

Atmospheric model

The atmospheric component of MCMS, the Weather Research and Forecasting (WRF) model, is developed in the National Center for Atmospheric Research (NCAR) in association with the National Oceanic and Atmospheric Administration (NOAA), the National Center for Environmental Prediction (NCEP), and various other agencies (www.mmm.ucar.edu/weather-research-and-forecasting-model). The MCMS utilizes the commonly used ARW core of WRF, which is widely employed for research and operational purposes. The model uses the terrain-following hybrid sigma pressure as vertical coordinate and employs Arakawa C-grid for horizontal grid staggering. The model is customised with a single WRF domain with horizontal grid spacing of 9 km and 35 vertical sigma levels (Mandal et al. 2016). The model top is kept at 10 hPa and utilizes a number of physical parameterisation schemes for microphysics, cumulus convection, surface, planetary boundary layer, and atmospheric radiation in order to optimise the outputs as described by Mandal et al. (2016).

Ocean model

The ocean component of MCMS is the Regional Ocean Modelling System (ROMS). It is a split-explicit, free-surface, 3-dimensional primitive equation oceanic model based on the non-linear terrain-following coordinate (www.myroms.org). ROMS employs short time steps to

advance the surface elevation and barotropic momentum equations, whereas much larger time step is used for advancement of temperature, salinity, and baroclinic momentum. It uses a third-order accurate predictor (Leap-Frog) and corrector (Adams-Molton) time-stepping algorithm for time discretisation (www.myroms.org). The higher resolution in the ocean mixed layer and bottom boundary layer is attained by means of the stretched terrain-following coordinates. Similar to ARW-WRF, the horizontal grid staggering in the ROMS model is based on Arakawa C-grid. ROMS allows vertical and horizontal advection schemes, and parameterisation for vertical and horizontal mixing. For simplicity, the ROMS grids are co-located with the ARW-WRF grids in order to avoid the remapping and grid-interpolation while transferring the prognostic variables between the model components. The southern and western boundaries are held open while the northern and eastern boundaries are closed, and the model uses 40 vertical σ levels, with vertical stretching parameters $\theta_b = 0.4$, $\theta_s = 7$, and $T_{cline} = 10$ m.

Coupling of the models

The Model Coupling Toolkit (MCT) is an advanced software tool written in Fortran90, which enables the efficient transmission of various prognostic variables between different components of the models, and supported by the parallelisation mechanism called Message Passing Interface (MPI) (www.mcs.anl.gov/research/projects/mct/). During coupled run, ROMS receives surface stresses and net-heat fluxes computed from ARW-WRF while it sends SST to the ARW-WRF; the time interval for variable transfer between component models is 600 s. The approach of forcing the ROMS model with momentum and heat fluxes directly computed from ARW-WRF ensures flux consistency, since each model computes turbulent fluxes based on different physical parameterisation schemes.

Data used

Daily optimum interpolation SST (OISST) products (available from www.esrl.noaa.gov) are used to study the TC-induced SST cooling and model validation. It combines microwave and infrared imageries from multiple satellite sensors to provide daily SST over the whole globe at a spatial resolution of 9 km. The microwave SSTs

are derived from Tropical Rainfall Measuring Mission’s (TRMM) Microwave Imager (TMI) and Advanced Microwave Scanning Radiometer—Earth Observing System (AMSR-E), AMSR2 and WindSat sensors, while infrared SSTs are obtained from MODIS observations.

Sea surface height anomaly (SSHA) and surface geostrophic currents are obtained from Archiving, Validation and Interpretation of Satellite Oceanographic (AVISO) (www.aviso.altimetry.fr). These data are prepared by combining sea level observations from multi-mission altimeters such as Saral/Altika, Jason-1, Jason-2, ENVISAT, Cryosat-2, GFO, ERS1/2, and TOPEX/Poseidon (www.aviso.altimetry.fr/en/data/). This study uses daily (8–13 Oct. 2013 and 7–12 Oct. 2014) SSHA and geostrophic current available at a spatial horizontal resolution of $1/4^\circ \times 1/4^\circ$.

We have also used Argo temperature and salinity profiles to examine the post-cyclone recovery of the ocean. The Argo data are obtained from CORIOLIS (www.coriolis.eu.org), which provides in situ data acquisition service for global oceans. The quality of data obtained from various platforms is controlled within 24 h using internationally agreed procedures (www.coriolis.eu.org) and data is distributed to major ocean forecasting centres and research community for further use.

The initial and boundary conditions for both ARW-WRF and ROMS models are derived from the latest version of Climate Forecast System (CFSv2) operational analyses developed in NCEP. Six-hourly CFSv2-analysed products having 0.5° spatial resolution with 38 and 40 vertical levels for atmosphere and ocean respectively are used in this study. The details about the period of data used for different experiments are described in the ‘Numerical experiments’ section. Additionally, weekly chlorophyll a concentration from MODIS Aqua (modis.gsfc.nasa.gov) for 30th September to 23rd October for years 2013 and 2014 is analysed. Daily optimally interpolated sea surface temperature (OISST) (www.esrl.noaa.gov) for the week of containing the TCs are used in this study.

Numerical experiments

Two experiments were performed using the coupled MCMS model, one for (a) Phailin and the other for (b) Hudhud.

a. Phailin simulation First, the ROMS model is spun up from 00 UTC of 1 September 2013 to 12 UTC of 8 October 2013 using the ocean initial conditions, boundary conditions, and atmospheric surface forcing fields from CFSv2. The spin up conditions generated are used as initial conditions for the coupled run at 12 UTC of 8 October 2013. Since the initial conditions for both the models are derived from NCEP-CFSv2 analysis, the model initial conditions retain the momentum and the thermodynamic balances between the ocean and atmosphere.

b. Hudhud simulation In this case, the ROMS model is spun up from 00 UTC of 1 September 2014 to 12 UTC of 7 October 2014 with ocean initial condition, boundary condition and atmospheric surface forcing fields derived from CFSv2. The initial condition for the ROMS model for the coupled run is derived from the spin up conditions at 12 UTC of 7 October 2014. The model setup for both atmosphere and ocean remains the same as that of the Phailin experiment.

Pre-storm ocean conditions over BoB and intensification of TC

Figures 1 a and c (b and d) illustrate pre-storm SST and tropical cyclone heat potential (TCHP) for Phailin as on 8 October 2013 (Hudhud as on 7 October 2014). The TCHP is calculated using the following equation:

$$TCHP = \int_{z_0}^{z_{26}} \rho C_p (T(z) - 26) dz \tag{1}$$

where C_p is the specific heat at constant pressure, ρ is the average density of ocean water, $T(z)$ is the temperature of the level dz , z_{26} is the depth of 26 °C isotherm, and z_0 is the surface.

It is very interesting to note that relatively higher SST is prevalent all over the Bay during the genesis of Hudhud as compared with that of Phailin. Simultaneously, the TCHP is found to be lower in the case of Hudhud compared with that of Phailin. Presence of high TCHP (up to 85 kJ/cm², Fig. 1c) in the central BoB indicates that large amount of energy is available for the TC to intensify (Wada 2015). To investigate more on the existence of high TCHP over the region, depth of 26 °C isotherm, mixed layer depth (MLD), and barrier layer

thicknesses (BLT) are investigated. Isothermal layer depth (ILD) is estimated as the depth at which temperature decreases by $0.8\text{ }^{\circ}\text{C}$ from SST (Kara et al. 2000). The MLD is estimated using a density-based criterion with a $0.8\text{ }^{\circ}\text{C}$ change in temperature as proposed by Kara et al. (2000). The difference between ILD and MLD represents the BLT. It is found that $26\text{ }^{\circ}\text{C}$ isotherm is present at shallow depth over the Bay during Hudhud as compared with Phailin (Fig. 1e, f). Also, shallow MLD less than 20 m is present in the west and northwest of BoB during both the cyclones (Fig. 2a, b), and is consistent with the findings of Wang and Han (2014). However, a deeper barrier layer is observed in the central and eastern BoB on 8 October 2013, during formation of TC Phailin (Fig. 2c). Presence of deeper thermocline in the pre-storm period made large amount of energy available for Phailin.

The daily minimum sea level pressure is used as proxy to describe the intensities of the cyclone. Figure 1c, d shows daily minimum sea level pressure at 12 UTC based on IMD best-track observations for Phailin, 8–13 October 2013 (for Hudhud, 7–12 October 2014) as one moves

from right to left in the figure. During 9–10 October 2013, Phailin passed over the area of high TCHP ($> 75\text{ kJ/cm}^2$) present in the northeastern and central BoB. Availability of high TCHP caused an increase in air-sea enthalpy flux from the ocean to the atmosphere (Balaguru et al. 2014) and consequently favoured storm intensification; thus, surface pressure dropped from 993 to 978 hPa. Subsequently, it encountered much higher TCHP (ranging up to 85 kJ/cm^2) in the central BoB and undergone rapid intensification (pressure drop from 978 to 939 hPa) in a very short span of its life cycle (10–11 October 2013). A detailed study on effect of TCHP and TC intensity is described in Wada (2015). Upon passing over the area of lower TCHP ($\sim 45\text{ kJ/cm}^2$) present in the western bay, the storm stumbled and its intensity reduced. Along with the upper-ocean conditions, the presence of mesoscale features like eddies, fronts, and rings can affect the intensity of TC and its track (Walker et al. 2005; Scharroo et al. 2005; Zheng et al. 2008, 2010). In order to investigate the presence of eddies along the cyclone track, we analysed the SSHA over the region. Figures 3 a and b display SSHA over the BoB on 8 October 2013 (for Phailin) and 7

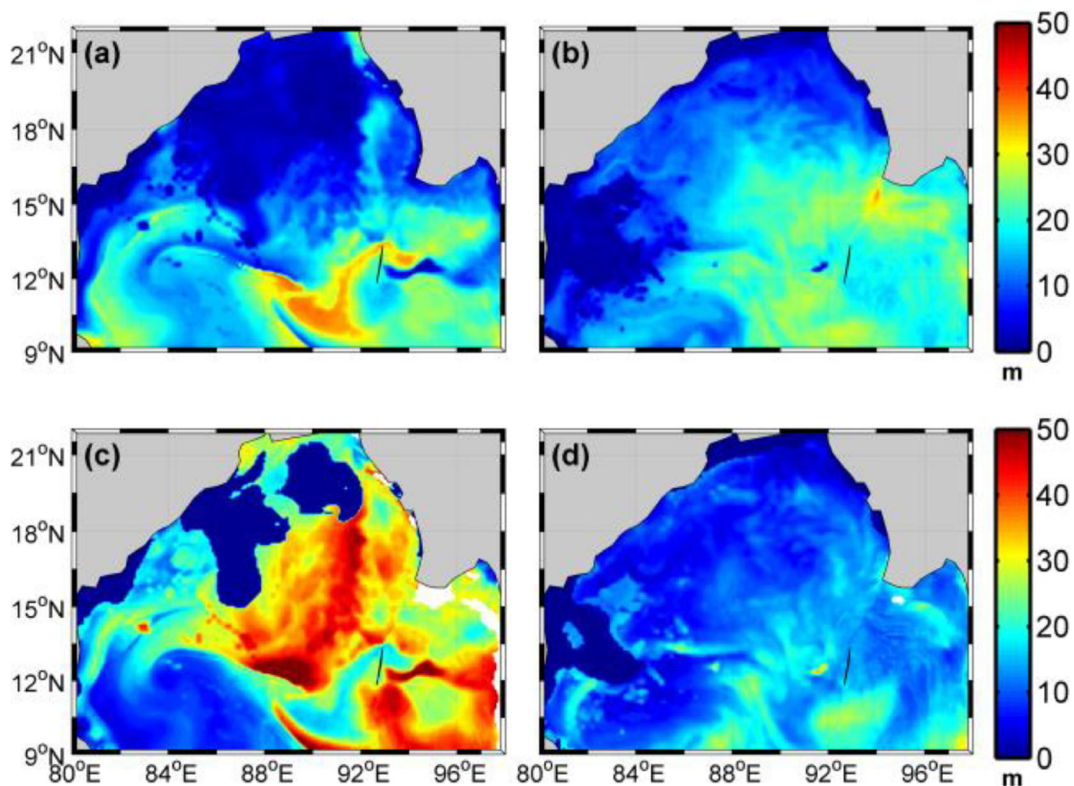


Fig. 2 Pre-storm (a) mixed layer depth and (c) barrier layer thickness on 8 October 2013 for Phailin; (b) and (d) are same as (a) and (c) but for Hudhud on 7 October 2014

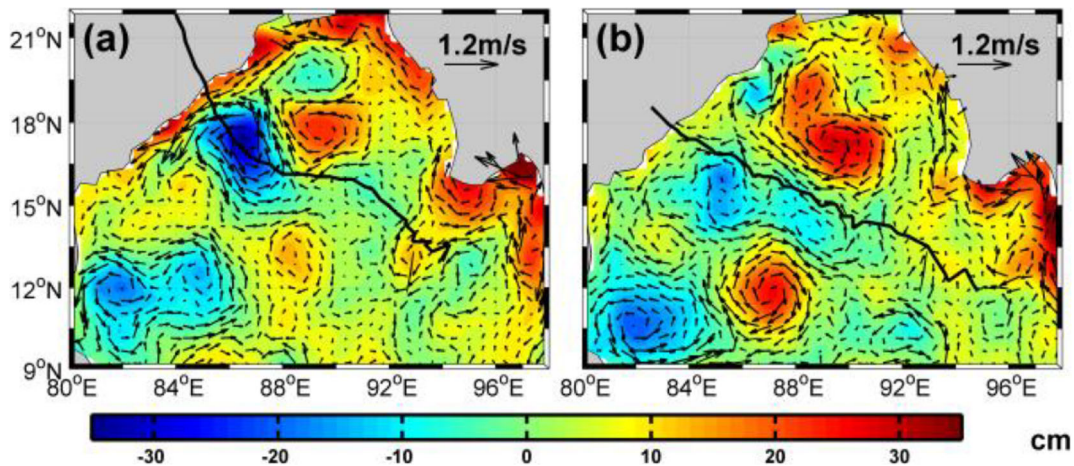


Fig. 3 SSHA (shaded) and geostrophic currents (vector) as on (a) 8 October 2013 for Phailin and (b) 7 October 2014 for Hudhud. Respective storm tracks are overlaid on it

October 2014 (for Hudhud) respectively. It is interesting to note the presence of a cold core eddy (CCE) (SSHA -33 cm) centred around 17° N and 86° E on 8 October 2013 (Fig. 3a). The CCE is accompanied with strong cyclonic vorticity (fig. S1). Further, to investigate feature of CCE in the region, the MCMS-simulated upper surface currents averaged for top 100 m and the depth of 26° C isotherm are examined. The averaged current for the top 100 m indicates the presence of cyclonic eddy associated with the shallow isotherms (ILD as seen in Fig. 1e). It is found that the eddy was almost stationary during Phailin (figure not shown). The track of Phailin shows that it encountered the CCE in northeastern BoB before its landfall. It is to be

noted that the region of low TCHP matches with the location of CCE. The presence of CCE reduces the moisture influx to the TC, hence reducing the intensity of the cyclone before its landfall.

On the other hand, prior to the passage of Hudhud, on 7 October 2014, presence of a weak (compared with the CCE present during Phailin) CCE (SSHA -20 cm) is noticed in SSHA, and geostrophic currents (Fig. 3b) and Okubo-Weiss parameter (fig. S1). However, shallower 26° C isotherm is prominent to the left of the Hudhud track. Nevertheless, Hudhud with its slow translation speed on 11 October 2014 (Fig. 4) draws sufficient energy from the underlying ocean despite exposed to relatively low TCHP.

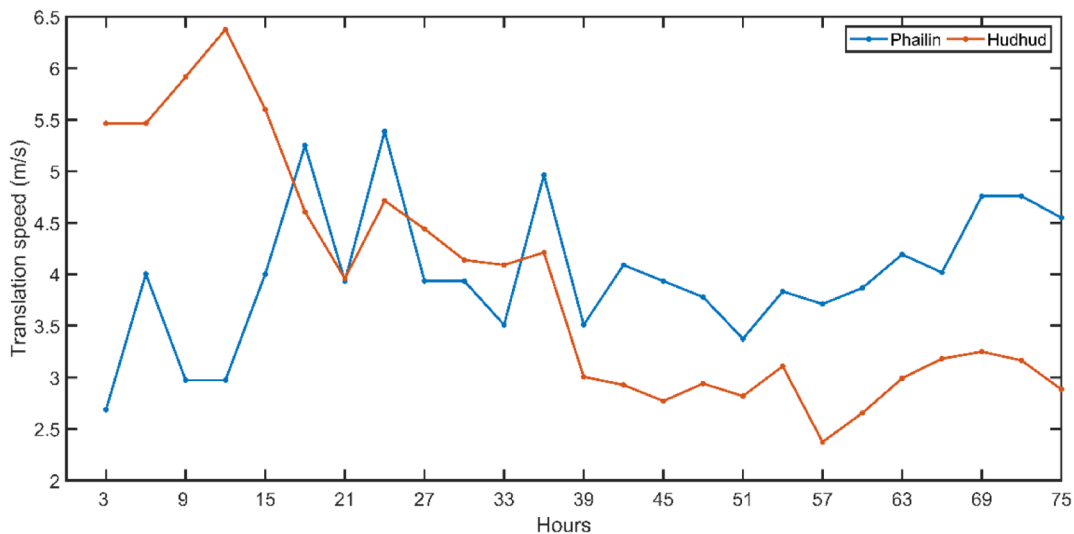


Fig. 4 Translation speed of Phailin (12 UTC 08 October to 15 UTC 11 October 2013) and Hudhud (12 UTC 07 October to 15 UTC 10 October 2014)

Upper-ocean response to TC passage

It will be interesting to examine the reaction of ocean surface to the passage of TC. SST drops in 12 October 2013 (for Phailin) and 13 October 2014 (for Hudhud) are estimated after 6 h of landfall using MCMS simulations and OISST (Fig. 5). Generally, strong wind is present at the right side of the storm track in the Northern Hemisphere, which induces asymmetry in SST cooling. Strong SST cooling of 4.6 °C (for Phailin) and 5.2 °C (for Hudhud) is observed at the right side of the storm track (Fig. 5). Comparison of model results with OISST correlated well providing the evidences of anomalous strong cooling in both the cases as observed in the CCE locations. The presence of a thick barrier layer (~ 45 m) during Phailin (Fig. 2c) did not allow mixing of subsurface water in the bay. The observation also showed that the cyclone Phailin could not be able to break the barrier layer and the mixing is confined to the

upper surface of the ocean only (Chaudhuri et al. 2019). A similar response of the upper ocean is reported during cyclone Sidr (Vissa et al. 2013). However, the presence of cyclonic eddy enhanced the cooling process in the northwestern bay. Thus, a significant drop in SST is noticed at the CCE location both in observation and model simulations (Fig. 5a, b). Similar results have been reported by Qiu et al. (2019) for Phailin. In contrast, weak stratification and shallow BL (~ 17 m) along with slower translational speed (~ 3 m/s) (Fig. 4) of Hudhud promoted mixing and reduced SST over an extended area of the bay along the track of the cyclone (Fig. 5).

Furthermore, to examine the influence of TC on subsurface cooling, we analyse the model-simulated temperature and salinity profiles at three different locations present to the right of the storm tracks, referred as A, B, and C as shown in Figs. 5 a and c. Notably, the locations A, B, and C possess high, medium, and low surface cooling

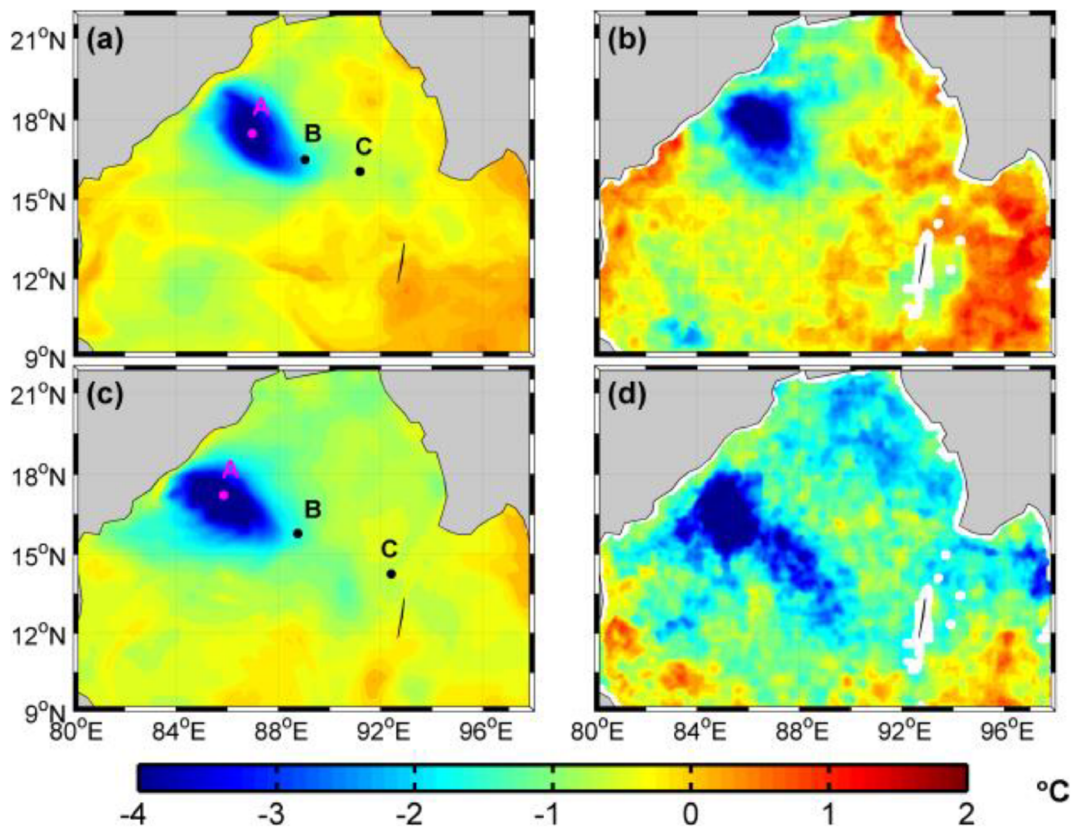


Fig. 5 Sea surface temperature difference: (a) simulated by MCMS and (b) OISST on 12 October 2013 for Phailin. (c) and (d) are same as (a) and (b) but relevant to 13 October 2014 for Hudhud. A, B, and C are the locations at the right-side of storm

track used for analysis (refer to the 'Pre-storm ocean conditions over BoB and intensification of TC' and 'Upper-ocean response to TC passage' sections)

as seen in SSTA for both the TCs (Fig. 5b, d). Figures 6 and 7 present evolution of temperature and salinity in the upper 100 m of the ocean surface at 12 UTC of each day at above three locations for the entire life span of Phailin and Hudhud respectively.

As Phailin passes over the location ‘C’ on 9 October 2013, it encountered strong stratified upper ocean. Cooling of the upper ocean starts due to shear induced turbulent mixing (Fig. 6c). But, the SST cooling is low (~ 0.75 °C) due to the presence of thick thermocline and low intensity (980 hPa) of the storm. Furthermore, the presence of a strong stratified layer at the upper surface of the ocean reduces the effect of TC-induced SST cooling. Similar results are found by Qiu et al. (2019) and Chaudhuri et al. (2019). Further, availability of high TCHP and reduced negative SST feedback (i.e., TC-induced SST cooling) corroborates with the rapid intensification phase of Phailin. As TC passed over the location ‘B’ on 10

October 2013, it became intense, thus enhancing the shear stress on the ocean surface and turbulence mixing as well. It is clearly seen in the model simulation with the cold, salty water coming to the surface after advent of the TC on 10 October 2013. Figure 6a shows severe upwelling of cold thermocline water of less than 25 °C during and after the storm passes over the location ‘A’. This could be attributed to the combined effect of upwelling due to the presence of CCE at location ‘A’ and the cyclone-induced turbulent mixing. Thus, the presence of CCE enhanced the cyclone-induced surface cooling.

Conversely, Hudhud was a low-intense cyclone compared with Phailin and associated with low TCHP over the whole basin. At location ‘C’, the storm Hudhud was unable to disturb the thermocline during the passage though shallow thermocline is present (Fig. 7c, f). But, by the time the storm passes over the location ‘B’, it was intensified. The increase in storm intensity enhanced shear induced vertical mixing and broken the shallow

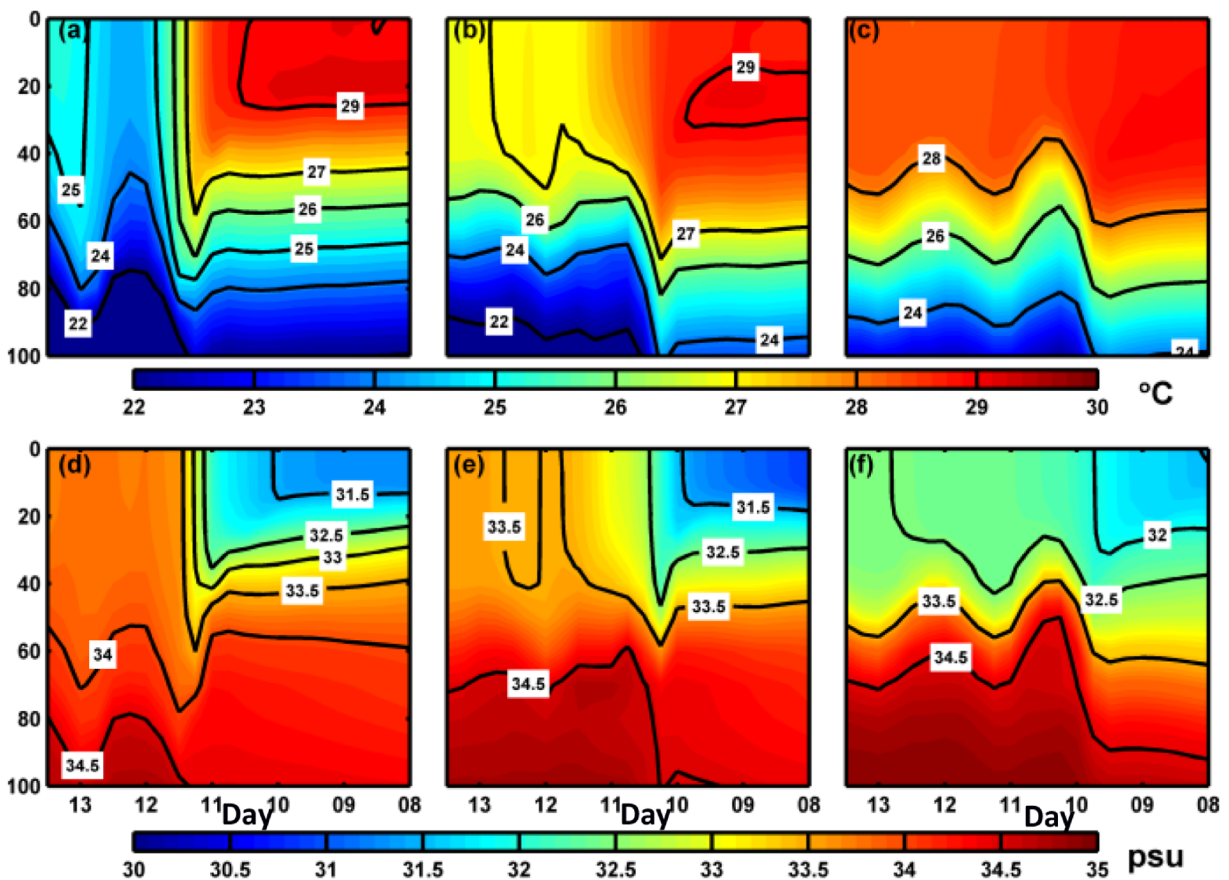


Fig. 6 Temperature profile at 12 UTC versus day in October 2013 at (a) location A, (b) location B, and (c) location C (shown in Fig. 4) and salinity profile at 12 UTC versus day in October

2013 at (e) location A, (f) location B, and (g) location C for Phailin. The *x*-axis represents the ‘day’ and the *y*-axis represents the ‘depth’

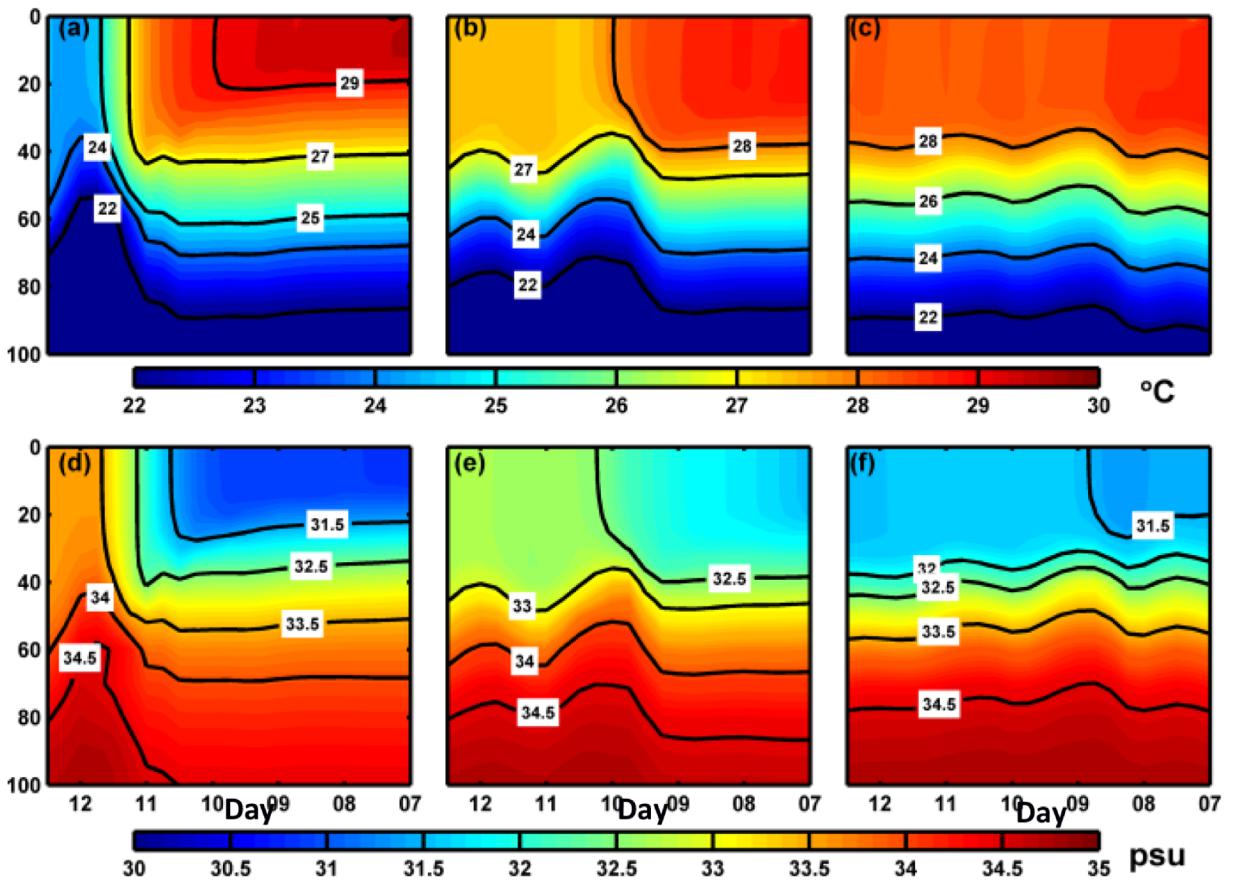


Fig. 7 Temperature profile at 12 UTC versus day in October 2013 at (a) location A, (b) location B, and (c) location C (shown in Fig. 4) and salinity profile at 12 UTC versus day in October

2013 at (e) location A, (f) location B, and (g) location C for Hudhud. The x-axis represents the ‘day’ and the y-axis represents the ‘depth’

thermocline present over the region and brought cold, dense, high saline water to the surface and resulted in surface cooling (Fig. 7b, g). Sluggish movement of the storm allows to receive more moisture from the ocean surface and increases its intensity; also, it results in reduction in SST along the storm track. The SST cooling is maximum at location A. It is attributed to the combined effect of upwelling due to the CCE in the region and the cyclone-induced vertical mixing (Fig. 7a, d).

To examine the SST cooling further, we analyse the temperature tendency for both the cyclones. The temperature tendency is defined as the rate of change of temperature caused by advection, mixing and upwelling/downwelling, and surface radiative and turbulent heat flux and is expressed as

$$\frac{\partial T}{\partial t} = -u\left(\frac{\partial T}{\partial x}\right) - v\left(\frac{\partial T}{\partial y}\right) - w\left(\frac{\partial T}{\partial z}\right) + \left(\frac{dT}{dt}\right) \quad (2)$$

Figure 8 presents the daily temperature tendency for active 3 days of both the cyclones (10, 11, and 12 October). It is to be noted that by 10 October, Hudhud acquired enough energy and the intensity was similar to that of Phailin. Interestingly, the temperature tendency for Phailin shows strong cooling over the region, right of the storm track (Fig. 8b), on 11 October 2013, which the storm crosses one day before. Well-spread cooling nearer to the coast noticed on 12 October 2013 (Fig. 8c) could be the combined effect of the presence of CCE and the TC-induced upwelling. Increased storm intensity and presence of shallow barrier layer favoured the upper-ocean mixing. However, Hudhud shows widespread cooling on 11 October 2014, compared with that of Phailin on 11 October 2013 (Fig. 8(b), (e)). Though Hudhud is relatively weaker in intensity than the Phailin (centre pressure is less by 10 hPa), the presence of shallower

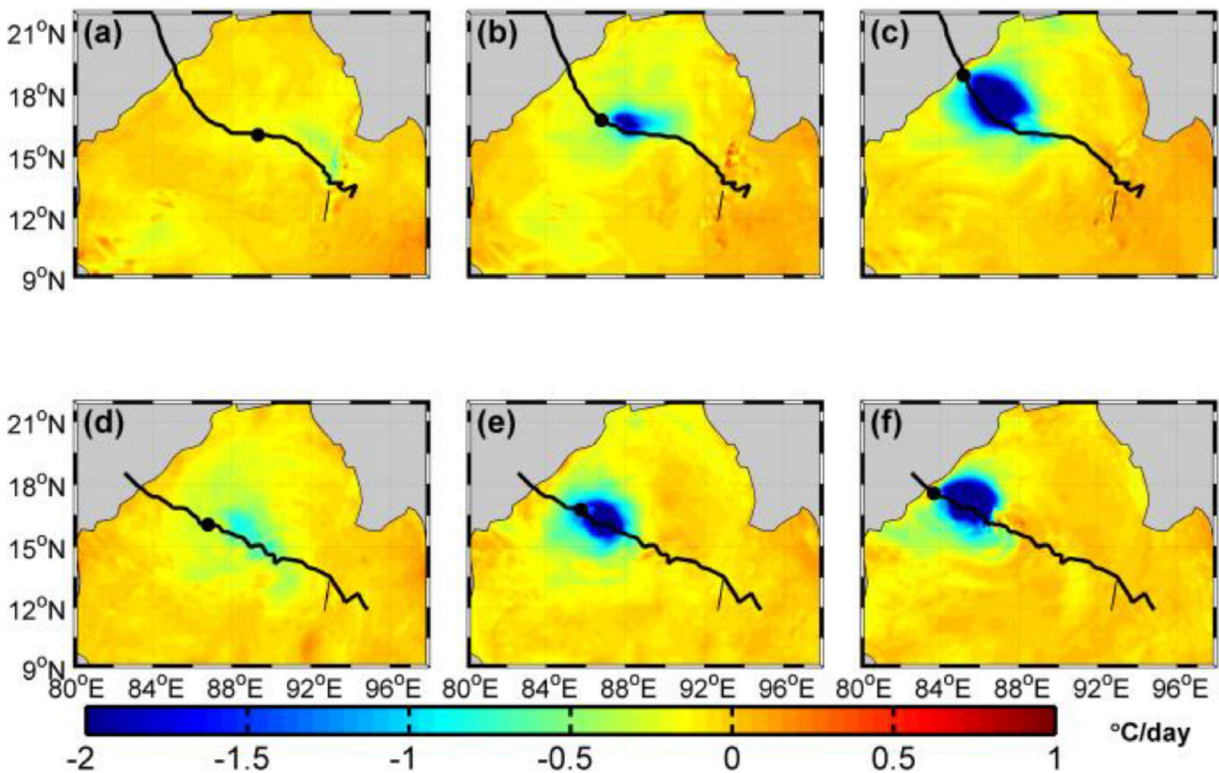


Fig. 8 Temperature tendency at 12 UTC relevant for Phailin on October (a) 10, (b) 11, and (c) 12. (d), (e), and (f) are the same as (a), (b), and (c) but during Hudhud. The cyclone track is superimposed. The black dots denote the location of the storm on the respective days

BLT enhanced SST cooling. The surface cooling seen on 12 October 2014 (Fig. 8(f)) is a combined effect of the presence of CCE and TC-induced upwelling over the region. Thus, the upper ocean experiences similar responses with anomalous tendency in temperature after the passage of both the storms adjacent to the CCE on the third and fourth days. The analysis clearly brings out the significant influence of pre-existing upper-ocean state on SST cooling.

Dynamical upper-ocean response to the TC

For steady state, zonal (v_E) and meridional (u_E) Ekman transports and Ekman pumping are defined in Eqs. (3) and (4) respectively following Wang and Han (2014).

$$u_E = \frac{\tau_{yo}}{\rho_o f}, \quad v_E = \frac{-\tau_{xo}}{\rho_o f} \tag{3}$$

Ekman pumping velocity (ω_e),

$$\omega_e = \frac{\partial}{\partial x} \left(\frac{\tau_{yo}}{\rho_o f} \right) - \frac{\partial}{\partial y} \left(\frac{\tau_{xo}}{\rho_o f} \right) \tag{4}$$

where τ_{xo} and τ_{yo} are the surface stress along the x -axis and y -axis respectively, ρ_o is the density of ocean water, and f is the Coriolis parameter.

Figures 9 displays 3 days averaged surface wind stress, Ekman pumping (shaded) and Ekman transport (vector), mean ocean temperature (T_{100}) (shaded), and current (vector) for top 100 m for 9–11 October and 11–13 October 2013 for Phailin. The wind stress, Ekman pumping, and Ekman transport observed around the storm centre adhere to intensification of Phailin during 9–11 October 2013 and are shown in Figs. 9 (a) and (b). The surface Ekman divergence-induced upwelling exceeds 0.4 mm/s, whereas Ekman convergence decays radially outward from the storm centre and induces surface convergence in the adjoining northeastern side. Reduction in Ekman transport away from the storm centre results in Ekman convergence and causes downwelling of surface water (0.4 mm/s or less) (Fig.

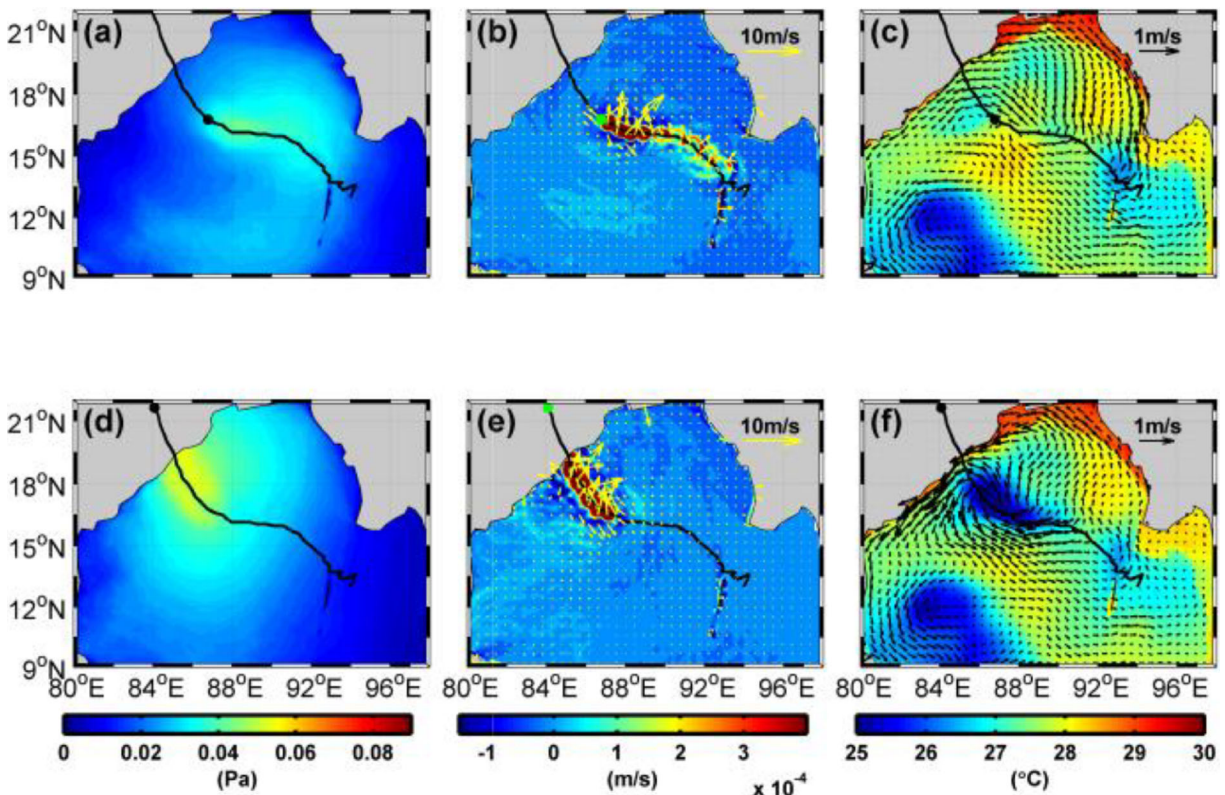


Fig. 9 Averaged (a) wind stress, (b) Ekman pumping (shaded) and transport (vector), and (c) mean temperature (shaded) and current (vector) for upper 100 m for the period of 9–11 October

9b). The upper-ocean cooling response is not significant over the observed Ekman divergence during 9–11 October 2013. However, cool upsurge of subsurface waters is noticed over the wake regions (Fig. 9c). During 11–13 October 2013, strong wind stress (Fig. 9d) and adjoining coastal effect results in increased spatial spread of Ekman upwelling as seen in Fig. 9e. Consequently, the effect of upwelling associated with CCE and advection reduces the upper 100-m temperature to nearly 25 °C in the remnant wake of cyclone Phailin as shown in Figs. 6a and 9f.

Figure 10 displays the same for 8–10 October and 10–12 October 2014 for Hudhud. Lower storm intensity, as evident from wind stress (Fig. 10a), induced relatively low Ekman pumping of 0.2 mm/s (average) in the initial period of cyclone (Fig. 10b), whereas enhanced upwelling is observed for the period 10–12 October (0.4 mm/s and above) due to increased wind stress (Fig. 10d) and adjoining coastal effect. Ekman convergence is relatively higher at the left quadrant of the storm track (maximum Ekman pumping 0.4 mm/s

during Phailin. Plots (d), (e), and (f) represent the same as (a), (b), and (c) respectively but for the period of 11–13 October. Storm track is superimposed

(Fig. 10e)). This can be attributed to the low translation speed (Fig. 4) and observed leftward bias in the storm wind stress.

Upwelling influenced by TC winds causes subsurface mixing outward to the radius of maximum wind and elevates vigorous doming of cool thermocline water inward to it. Immediate response is reflected in the ocean currents due to associated surface stress while, the subsurface isotherms responded with a 24-h lag. This is attributed to the easier exchange of momentum (i.e., frictional stress) in fluid than that of kinetic energy (Pond and Pickard 1983). In addition, it takes a considerable amount of time for the mechanical energy imparted by the surface stress to reach deeper isotherms in order to promote upwelling. Since significant mixing occurs at 26 °C isotherm, 23 °C isotherm is used as reference for this analysis. The change in isotherm depth is calculated using Eq. (5).

$$\frac{\partial(\text{ILD})}{\partial t} = \frac{\text{ILD}(t) - \text{ILD}(t - \Delta t)}{\Delta t} \quad (5)$$

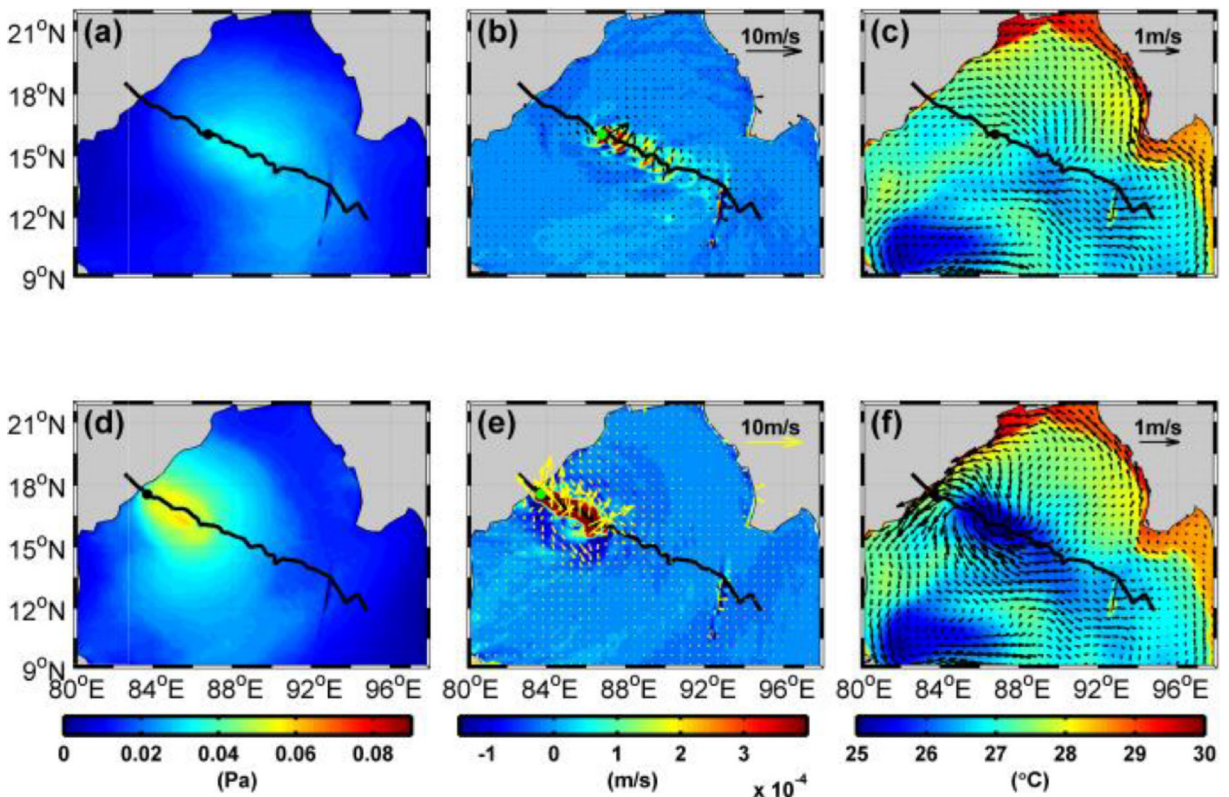


Fig. 10 Averaged (a) wind stress, (b) Ekman pumping (shaded) and transport (vector), and (c) mean temperature (shaded) and current (vector) for upper 100 m for the period of 8–10 October

during Hudhud. Plots (d), (e), and (f) represent the same as (a), (b), and (c) respectively but for the period of 11–13 October. Storm track is superimposed

Considering the prominent effect of upwelling that occurred at a 24-h lag of the storm passage over any particular region, investigation of upwelling, based on isotherm displacement averaged over an azimuthal area of 2° radii from storm centre, is carried out for both the TCs at 12 UTC and presented in Table 1. Phailin passage shows a maximum upwelling of 62 cm/h (Table 1) on 12 October 2013 that coincides with the location of CCE where maximum SST cooling of 4.2 °C is observed (Fig. 10(c)). However, during Hudhud passage, the upper ocean

exhibits a maximum upwelling of 43 cm/h (Table 1) prior to the location of CCE due to slow transition speed of storm.

To investigate changes in surface mesoscale features by the passage of cyclones, daily merged SSHA fields are analysed. Figures 11 and 12 present daily negative SSHA anomalies for Phailin and Hudhud cyclones respectively. The CCE prominently marked by negative SSHA (~ 1.5 cm) before the storm approaches the eddy on 10 October 2013. Southwestward boundary currents associated with secondary circulation of Phailin intensified the CCE. Further, on 11 October 2013, as Phailin approaches the eddy, cyclonic circulation is enhanced and the CCE deepens at its core. Subsequent increase in the strength of CCE is observed and reflected in SSHA (i.e., 12–13 October 2013) (Fig. 11). The change in CCE after the passage of Phailin signifies the dynamic response supported by inertial currents accompanied by the cold-wake region. In contrast to Phailin, weaker negative SSHA is located to the left of the Hudhud track (Fig. 12). Although gradual

Table 1 Average upwelling during Phailin and Hudhud

TC Phailin		TC Hudhud	
Date (at 12 UTC)	Upwelling (cm/h)	Date (at 12 UTC)	Upwelling (cm/h)
10/10/2013	32	10/10/2014	35
11/10/2013	44	11/10/2014	43
12/10/2013	62	12/10/2014	30

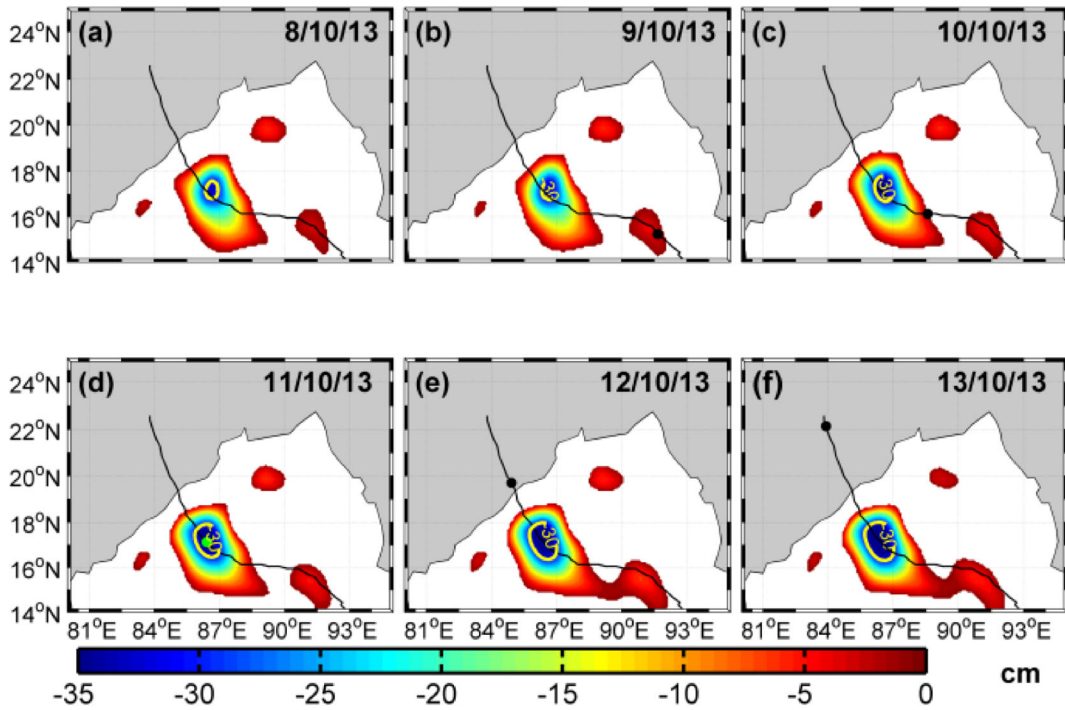


Fig. 11 SSHA at 21 UTC (a) 8, (b) 9, (c) 10 (d) 11, (e) 12, and (f) 13 October 2013 during Phailin. The closed contour represents SSHA of 30 cm. Storm track is superimposed

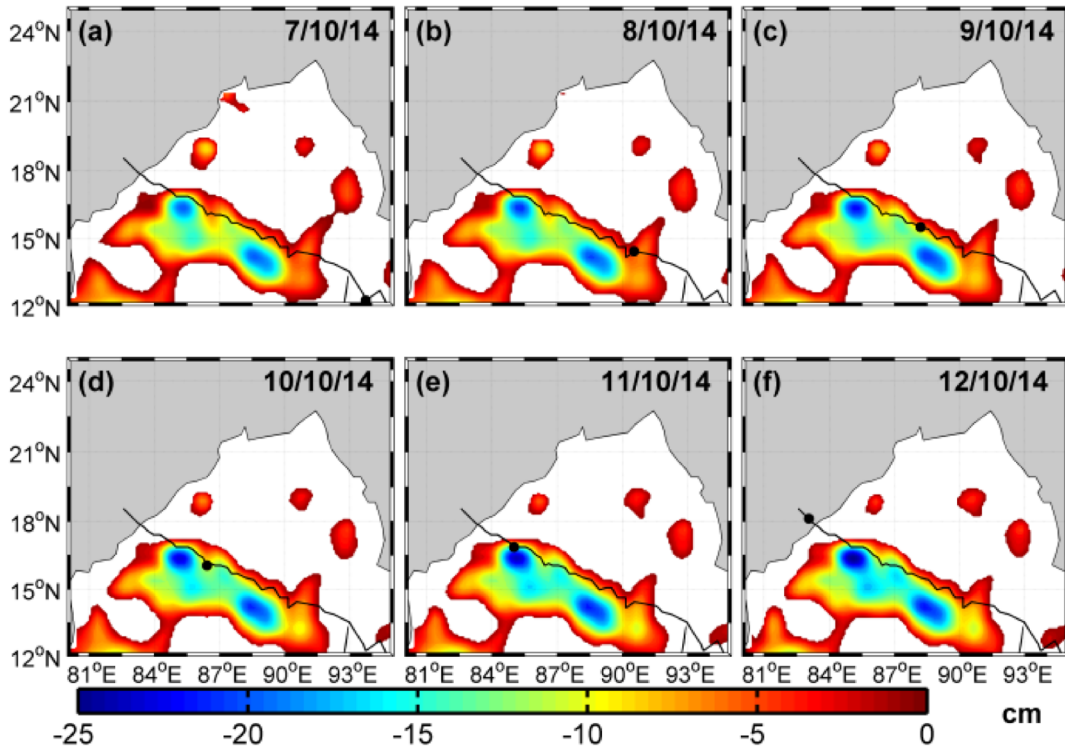


Fig. 12 SSHA at 21 UTC (a) 7, (b) 8, (c) 9 (d) 10, (e) 11, and (f) 12 October 2014 during Hudhud. Storm track is superimposed

increment in negative anomaly of SSHA is seen as Hudhud approaches the eddy on 10 October 2014, the variation in SSHA is less compared with Phailin (Figs. 11 and 12). The same is reflected in upwelling. However, the increase in spatial extent and strength of CCE is a less aftermath of the Hudhud passage, compared with that of Phailin. This is responsible for the discrepancy in upper-ocean response based on relative position of mesoscale features adjacent to the storm and storm intensity.

In addition to SST cooling, TC-induced upwelling brings up nutrient-rich water to the euphotic zone, thus stimulating biological production. Weekly mean chlorophyll a (Chl-a) concentration, derived from MODIS Aqua, is used to analyse chlorophyll bloom triggered by the cyclone. Figure 13 shows the weekly Chl-a concentration over the bay before (September 30 to October 7), during (October 8–15), and after (October 16–23) the passage of TCs Phailin and Hudhud. Co-location of the observed Chl-a bloom and CCE location implies the critical role of the CCE in upwelling and bloom. The absence of Chl-a

concentration in the images could be referred as the cloud cover regions (Fig. 13a–c). However, high Chl-a concentration patches are noticed in the weekly chlorophyll map after dissipation of Phailin (Fig. 13c). Nevertheless, a substantial bloom of Chl-a is noted at the trailing path of Hudhud, with maximum spread over the CCE region (Fig. 13e, f). In the region between 12° N–18° N and 82.5° E–90° E, average Chl-a concentration increases from 0.2 mg/m³ (pre-storm) to 0.7 mg/m³ after the passage of Hudhud. Lower stratification promotes entrainment of cold and nutrient-rich water from the subsurface and enhances Chl-a production even though upwelling is not so intense during the storm. Although Phailin is comparatively intense, the pre-existing cyclonic eddy favours the Chl-a bloom and the shear generated by the cyclone boosts upwelling for following week after the landfall of storm (Fig. 13c). However, scarcity of observations during TCs due to cloud coverage limits the study and comparison of Chl-a enhancement triggered by both the cyclones.

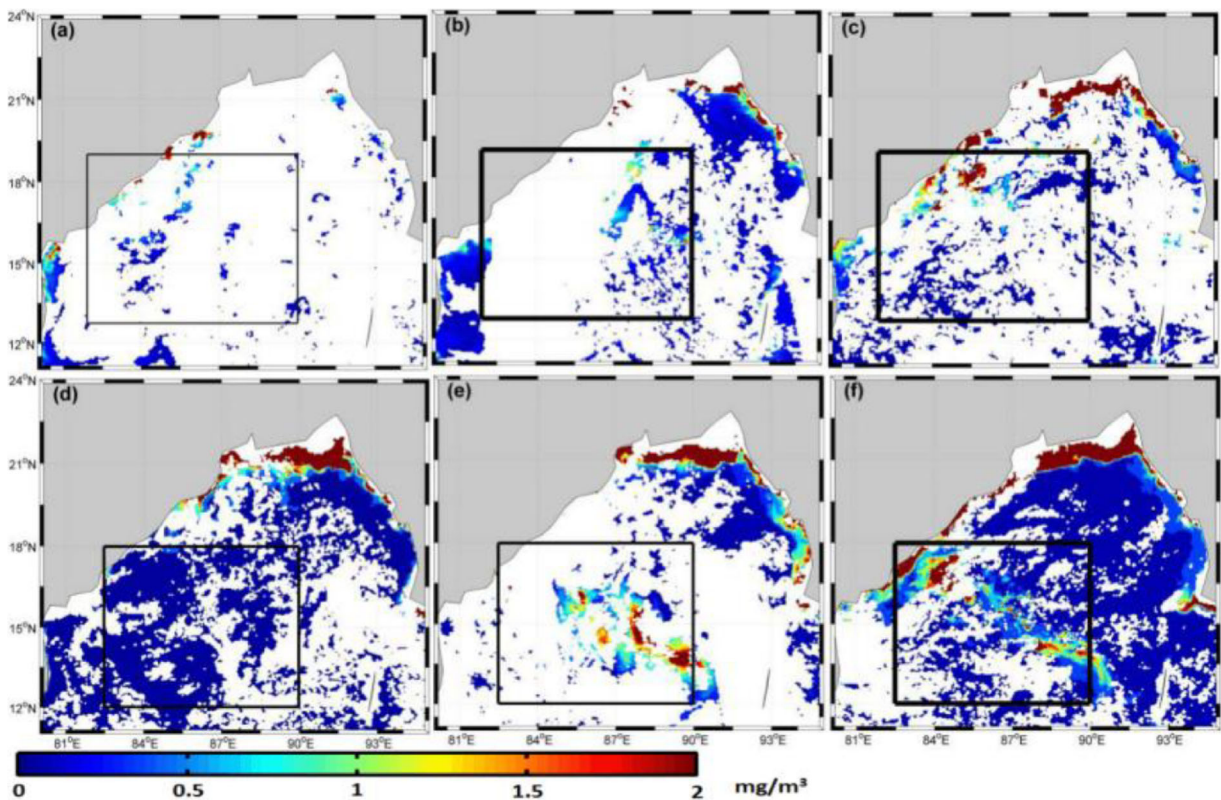


Fig. 13 Chl-a concentration in the BoB (a) a week before (September 30 to October 7 2013), (b) during TC (October 8–15, 2013), and (c) a week after dissipation of the storm (October 16–

23,2013) for Phailin. (d), (e), and (f) represent the same as (a), (b), and (c), respectively, for Hudhud

Upper-ocean recovery

The upper-ocean recovery after the passage of TCs Phailin and Hudhud is studied based on stand-alone ROMS simulations, which reserves the same model setup as MCMS. The time required for upper-ocean recovery depends on various factors and may range from days to weeks. Nevertheless, the recovery period is a direct function of storm intensity and translation speed and plays a vital role in subsequent weather events like development of low pressure after the passage of cyclone.

Recovery of surface temperature is estimated as change in daily SST from corresponding 7 days mean SST. The SST anomaly is calculated over the domain, 10° N– 25° N and 80° E– 95° E, from ROMS simulations and OISST observations for both the cyclones (Fig. 14). From Figs. 14 a and b, it is evident that both ROMS and OISST show similar structure, however the model slightly under estimates the SST ($\sim 0.3^{\circ}$ C) for Hudhud. After the passage of storms, SST recovers roughly within a period of 6 days. In October 2013 the mean SST in the entire domain showed a quick recovery after the landfall of Phailin, however, it undergoes cooling thereafter prevalent to seasonal change.

The analysis of upper-ocean recovery is also carried out based on Argo profiles. For this purpose, we have collected the Argo profiles for October 2013 over BoB. 58 profiles adjacent to the storm track are considered and analysed. The location of Argo profiles are displayed in Fig. 15a. Temperature data from Argo profiles is collected up to a maximum depth of 500 m and linearly interpolated to standard depth levels. Daily mean temperature profile for the days when Argo

profiles are available over that location is plotted in Fig. 15b. Evolution of temperature based on the ROMS model is presented in Fig. 15c. Observational evidence shows as Phailin approaches the location surrounded by Argo on 10 October, vigorous shear induced mixing started, which resulted in cooling the upper ocean to 27° C. However, the ocean quickly recovers roughly within a week. Although the model simulation could catch the mixing processes and indicates cooling, the subsurface response to storm winds is weaker and recovery is significantly delayed. The analysis clearly indicates that cooling observed in the location is entirely due to entrainment-driven mixing, as seen in the previous section (Fig. 6b). Due to scarcity of Argo profiles, the analysis could not be carried for Hudhud.

Further, the upper-ocean recovery tendency in terms of average TCHP, salinity, and SSHA is investigated over the domain 10° – 25° N and 80° – 95° E using ROMS simulations for Phailin and Hudhud (Fig. 16). The ocean recovers to its initial state roughly within a week during both cyclones, but overshoots initial TCHP during Hudhud (Fig. 16(a)) due to variations in upper-ocean conditions (stronger warm core eddies on 7 October 2014 as shown in Fig. 3b). For the same region, Fig. 16(b) shows very slow recovery of subsurface salinity (10 m average) which increases up to 31.9 PSU during Phailin and Hudhud. Evolution of minimum negative SSHA during both the cyclones shows a similar trend as indicated in Fig. 16(c). The minimum SSHA, -43 cm (for Phailin) and -29 cm (for Hudhud) on 20 October, marked the passage of cyclones.

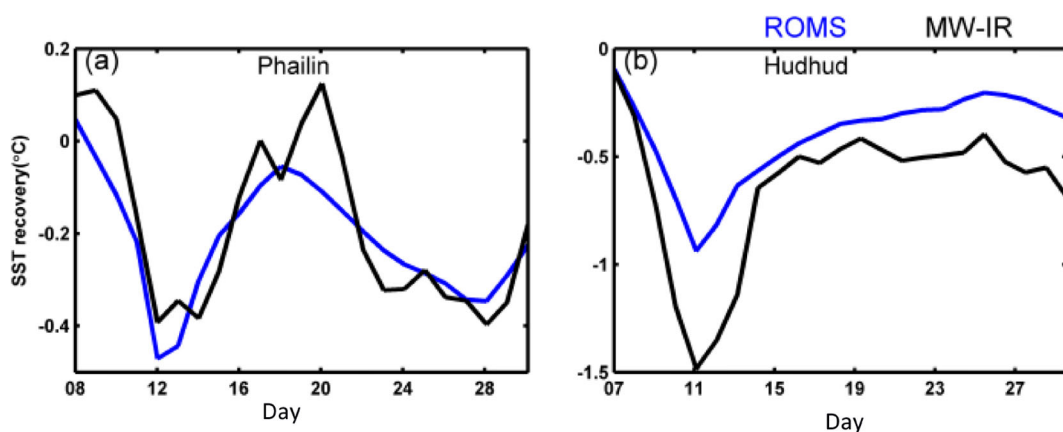


Fig. 14 Averaged SST over the domain (10° – 25° N and 80° – 95° E) versus the day, based on ROMS model and MW-IR observations for (a) Phailin (October 2013) and (b) Hudhud (October 2014)

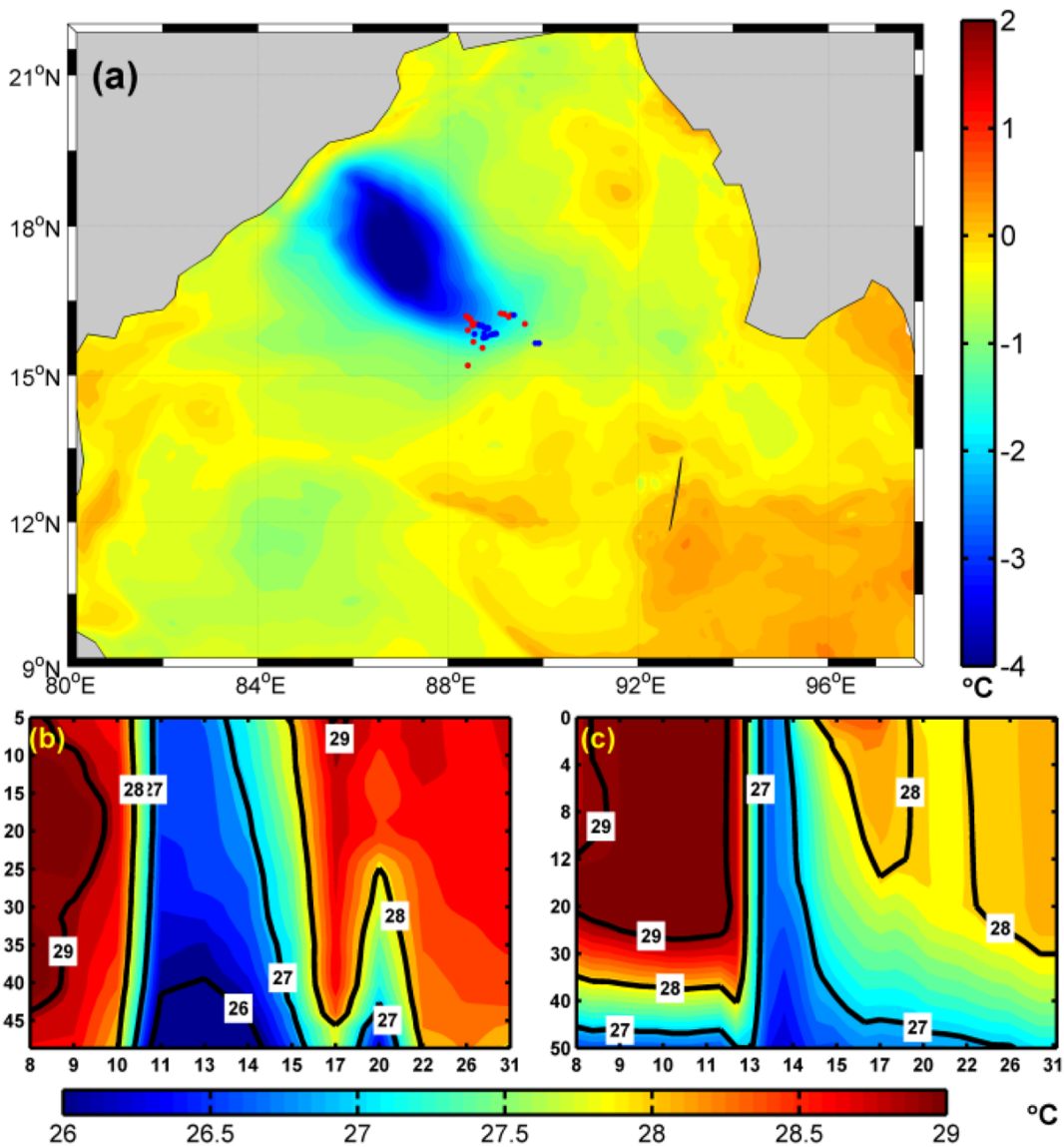


Fig. 15 (a) Location of Argo profiles in the background of SSTA for the month of October 2013 is marked. The blue and red marks signify the profiles that are available before and after storms

respectively. Temperature profile at position 89° E and 16° N versus day (b) averaged for all available Argo profiles and (c) based on ROMS model for the same date for Phailin

Summary

This study investigates the upper-ocean response during passage of two BoB post-monsoon cyclones, Phailin (in October 2013) and Hudhud (in October 2014), using a fully coupled atmosphere-ocean modelling system, MCMS. Analysis indicates that Phailin rapidly intensified as it moves over central BoB with a large TCHP closer to 85 kJ/cm². High TCHP is associated with deep isotherm layer accompanied by a thick barrier layer. Consequently, the storm-induced upper-ocean cooling

is subjected only to surface and mixed layer. However, the presence of strong CCE centred at 17° N and 86° E nearer to the storm track results in intense upwelling coupled with entrainment and upward doming of cold thermocline water. This reduces temperature of the upper ocean in the northwestern bay. The location of maximum SST cooling coincides with the position of pre-existing CCE. Associated shallow isotherm and lower TCHP over the eddy reinforce cooling tendency of the upper ocean. Maximum temperature tendency of - 4.21 °C/day on October 12, 2013, after Phailin moves

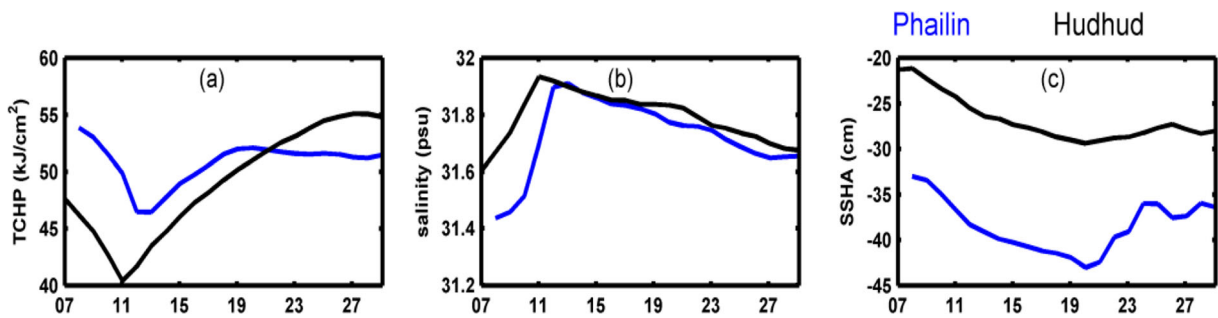


Fig. 16 Upper-ocean recovery over the domain (10–25° N and 80–95° E) based on ROMS model for the month of October after passage of Phailin (blue) and Hudhud (black) in terms of (a) TCHP, (b) subsurface salinity (10 m average), and (c) minimum SSHA

over the CCE is a clear indication of large negative feedback of the ocean that drastically reduces cyclone intensity.

Contrasting to this, during Hudhud, although SST in the basin is comparatively higher (initial > 1 °C than what is observed during Phailin), considerably less amount of heat is trapped in the upper ocean. Availability of less energy (TCHP < 50 kJ/cm²) over the bay is responsible for sluggish escalation in cyclone intensity during initial 3 days. Nonetheless, low translational speed of Hudhud from October 10 to 12 2014 over northwestern bay helps it to accumulate large energy from the ocean surface and developed to a severe cyclonic storm. Both the storms reach the category of very severe cyclonic storm owing to different dynamic processes and variations in pre-existing upper-ocean condition along their paths. Although shallow isotherm is prominent over the northwestern bay during Hudhud, the analysis of SSHA, geostrophic currents, and Okubo-Weiss parameter (not shown here) indicate considerably weak cyclonic eddy signature (with SSHA of – 20 cm) at the left quadrant of the storm track. Due to weaker CCE and its location to the left of the track, the impact of eddy in reducing upper ocean temperature is not so prominent. Considerably lower upwelling during Hudhud supports this finding.

Both cyclones show large reduction in SST after landfall. Although model simulations underestimate the observed SSTA, similar spatial extent is seen in both the cases. During Phailin, a highly asymmetric SSTA pattern is observed owing to its higher translational speed whereas considerable cooling occurs at the left of the track during Hudhud. Although both TCs show a quick recovery tendency, the upper ocean never returns to its initial state owing to the seasonal drop in temperature.

The dominance of different physical processes (horizontal advection, upwelling, etc.) in SST cooling during both cyclones is not included in this study and further analysis is necessary for clear understanding. Studies on upper-ocean recovery over BoB after passage of TCs are limited. But keeping in mind the consecutive TCs observed in BoB, this complex coupled ocean-atmosphere interactive process requires more attention from the scientific community.

Acknowledgments Daily optimum interpolation SST (OISST) and chlorophyll a (Chl-a) concentration are obtained from APDRC (<http://apdrc.soest.hawaii.edu/index.php>). The sea surface height and the geostrophic currents are provided by AVISO (<http://www.aviso.altimetry.fr/en/data/products/sea-surface-height-products/global.html>). Argo temperature data is obtained from CORIOLIS (<http://www.coriolis.eu.org/>). The initial and boundary condition for both ARW-WRF and ROMS model were derived from the latest version of Climate Forecast System (CFSv2) operational analyses developed in the NCEP.

References

- Balaguru, K., Taraphdar, S., Leung, L. R., & Foltz, G. R. (2014). Increase in the intensity of postmonsoon Bay of Bengal tropical cyclones. *Geophysical Research Letters*, *41*(10), 3594–3601.
- Bender, M. A., & Ginis, I. (2000). Real-case simulations of hurricane – ocean interaction using a high-resolution coupled model : effects on hurricane intensity. *Monthly Weather Review*, *128*, 917–946. [https://doi.org/10.1175/1520-0493\(2000\)128<0917:RCSOHO>2.0.CO;2](https://doi.org/10.1175/1520-0493(2000)128<0917:RCSOHO>2.0.CO;2).
- Bosart, L. F., Velden, C. S., Bracken, W. E., Molinari, J., & Black, P. G. (2000). Environmental influences on the rapid intensification of hurricane Opal (1995) over the Gulf of Mexico.

- Monthly Weather Review*, 128, 322–352. [https://doi.org/10.1175/1520-0493\(2000\)128<0322:EIOTRI>2.0.CO;2](https://doi.org/10.1175/1520-0493(2000)128<0322:EIOTRI>2.0.CO;2).
- Chan, J., Duan, Y., & Shay, L. (2001). Tropical cyclone intensity change from a simple ocean-atmosphere coupled model. *Journal of the Atmospheric Sciences*, 58, 154–172. [https://doi.org/10.1175/1520-0469\(2001\)0582.0.CO;2](https://doi.org/10.1175/1520-0469(2001)0582.0.CO;2).
- Chang, S., & Anthes, R. (1979). The mutual response of the tropical cyclone and the ocean. *Journal of Physical Oceanography*, 09, 128–135. [https://doi.org/10.1175/1520-0485\(1979\)009<0128:TMROTT>2.0.CO;2](https://doi.org/10.1175/1520-0485(1979)009<0128:TMROTT>2.0.CO;2).
- Chaudhuri, D., Sengupta, D., D'Asaro, E., Venkatesan, R., & Ravichandran, M. (2019). Response of the salinity-stratified Bay of Bengal to cyclone Phailin. *Journal of Physical Oceanography*, 49, 1121–1140. <https://doi.org/10.1175/JPO-D-18-0051.1> in press.
- Dare, R. A., & McBride, J. L. (2011). Sea surface temperature response to tropical cyclones. *Monthly Weather Review*, 139, 3798–3808. <https://doi.org/10.1175/MWR-D-10-05019.1>.
- Davis, C., et al. (2008). Prediction of landfalling hurricanes with the advanced hurricane WRF model. *Monthly Weather Review*, 136, 1990–2005. <https://doi.org/10.1175/2007MWR2085.1>.
- Demaria, M., & Kaplan, J. (1994). Sea-surface temperature and the maximum intensity of atlantic tropical cyclones. *Journal of Climate*, 7, 1324–1334. [https://doi.org/10.1175/15200442\(1994\)007<1324:SSTATM>2.0.CO;2](https://doi.org/10.1175/15200442(1994)007<1324:SSTATM>2.0.CO;2).
- Elsner, J. B., Strazzo, S. E., Jagger, T. H., Larow, T., & Zhao, M. (2013). Sensitivity of limiting hurricane intensity to SST in the Atlantic from observations and GCMs. *Journal of Climate*, 26, 5949–5957. <https://doi.org/10.1175/JCLI-D-12-00433.1>.
- Emanuel, K. A. (1986). An air-sea interaction theory for tropical cyclones. Part I: steady-state maintenance. *Journal of the Atmospheric Sciences*, 43, 585–604. [https://doi.org/10.1175/15200469\(1986\)043<0585:AASITF>2.0.CO2](https://doi.org/10.1175/15200469(1986)043<0585:AASITF>2.0.CO2).
- Gray, W. M. (1998). The formation of tropical cyclones. *Meteorology and Atmospheric Physics*, 67, 37–69.
- Jaimes, B., Shay, L. K., & Halliwell, G. R. (2011). The response of quasigeostrophic oceanic vortices to tropical cyclone forcing. *Journal of Physical Oceanography*, 41, 1965–1985. <https://doi.org/10.1175/JPO-D-11-06.1>.
- Kara, A. B., Rochford, P. A., & Hurlburt, H. E. (2000). An optimal definition for ocean mixed layer depth. *Journal of Geophysical Research*, 105, 16,803–16,821.
- Knaff, J. A., DeMaria, M., Sampson, C. R., Peak, J. E., Cummings, J., & Schubert, W. H. (2013). Upper oceanic energy response to tropical cyclone passage. *Journal of Climate*, 26, 2631–2650. <https://doi.org/10.1175/JCLI-D-12-00038.1>.
- Lin, Y.-L., Chen, S.-Y., & Hill, C. M. (2005). Control parameters for the influence of a mesoscale mountain range on cyclone track continuity and deflection. *Journal of the Atmospheric Sciences*, 62, 1849–1866.
- Lu, Z., Wang, G., & Shang, X. (2016). Response of a preexisting cyclonic ocean eddy to a typhoon. *Journal of Physical Oceanography*, 46, 2403–2410. <https://doi.org/10.1175/JPO-D-16-0040.1>.
- Mandal, M., Singh, K. S., Balaji, M., & Mohapatra, M. (2016). Performance of WRF-ARW model in real-time prediction of Bay of Bengal cyclone 'Phailin'. *Pure and Applied Geophysics*, 173, 1783–1801. <https://doi.org/10.1007/s00024-015-1206-7>.
- McPhaden, M. J., Foltz, G. R., Lee, T., Murty, V. S. N., Ravichandran, M., Vecchi, G. A., Vialard, J., Wiggert, J. D., & Yu, L. (2009). Ocean-atmosphere interactions during cyclone Nargis. *EOS (Washington, DC)*, 90, 53–54. <https://doi.org/10.1029/2009EO070001>.
- Neetu, S., Lengaigne, M., Vincent, E. M., Vialard, J., Madec, G., Samson, G., Kumar, M. R. R., & Durand, F. (2012). Influence of upper-ocean stratification on tropical cyclone-induced surface cooling in the Bay of Bengal. *Journal of Geophysical Research, Oceans*, 117, 1–19. <https://doi.org/10.1029/2012JC008433>.
- Palmen, E. (1948). On the formation and structure of tropical hurricanes. *Geophysica*, 3, 26–38 551.515.2, 551.587.
- Patnaik, K. V. K. R. K., Maneesha, K., Sadhuram, Y., Prasad, K. V. S. R., Ramana Murty, T. V., & Brahmananda Rao, V. (2014). East India coastal current induced eddies and their interaction with tropical storms over Bay of Bengal. *Journal of Operational Oceanography*, 7, 58–68. <https://doi.org/10.1080/1755876X.2014.11020153>.
- Petrova, L. I. (2010). Estimating the maximum potential intensity of tropical cyclones. *Russian Meteorology and Hydrology*, 35, 371–377. <https://doi.org/10.3103/S1068373910060026>.
- Pond, S., & Pickard, G. L. (1983). *Introductory dynamical oceanography* (p. 349). Oxford: Elsevier Butterworth-Heinemann.
- Qiu, Y., Han, W., Lin, X., West, B., Li, Y., Xing, W., Zhang, X., Arulananthan, K., & Guo, X. (2019). Upper ocean response to the super tropical cyclone Phailin (2013) over the freshwater region of the Bay of Bengal. *Journal of Physical Oceanography*, 49, 1201–1228. <https://doi.org/10.1175/JPO-D-18-0228.1>.
- Riehl, H. (1950). A model of hurricane formation. *Journal of Applied Physics*, 21, 917–925. <https://doi.org/10.1063/1.1699784>.
- Sadhuram, Y., Rao, B. P., Rao, D. P., Shastri, P. N. M., & Subrahmanyam, M. V. (2004). Seasonal variability of cyclone heat potential in the Bay of Bengal. *Natural Hazards*, 32, 191–209. <https://doi.org/10.1023/B:NHAZ.0000031313.43492.a8>.
- Scharroo, R., Smith, W. H. F., & Lillibridge, J. L. (2005). Satellite altimetry and the intensification of Hurricane Katrina. *EOS. Transactions of the American Geophysical Union*, 86, 366. <https://doi.org/10.1029/2005EO400004>.
- Shay, L. K., & Uhlhorn, E. W. (2008). Loop current response to hurricanes Isidore and Lili. *Monthly Weather Review*, 136, 3248–3274. <https://doi.org/10.1175/2007MWR2169.1>.
- Shay, L. K., Goni, G. J., & Black, P. G. (2000). Effects of a warm oceanic feature on hurricane opal. *Monthly Weather Review*, 128, 1366–1383. [https://doi.org/10.1175/1520-0493\(2000\)128<1366:EOAWOF>2.0.CO;2](https://doi.org/10.1175/1520-0493(2000)128<1366:EOAWOF>2.0.CO;2).
- Sun, D., Ritesh, G., Guido, C., Zafer, B., & Menas, K. (2006). Satellite altimetry and the intensification of hurricane Katrina. *EOS. Transactions of the American Geophysical Union*, 87(8).
- Sun, L., Li, Y. X., Yang, Y. J., Wu, Q., Chen, X. T., Li, Q. Y., Bin Li, Y., & Xian, T. (2014). Effects of super typhoons on cyclonic ocean eddies in the western North Pacific: a satellite data-based evaluation between 2000 and 2008. *Journal of Geophysical Research, Oceans*, 119, 5585–5598. <https://doi.org/10.1002/2013JC009575>.

- Tuleya, R. E., & Kurihara, Y. (1982). A note on the sea surface temperature sensitivity of a numerical model of tropical storm genesis. *Monthly Weather Review*, *110*, 2063–2069. [https://doi.org/10.1175/1520-0493\(1982\)110<2063:ANOTSS>2.0.CO;2](https://doi.org/10.1175/1520-0493(1982)110<2063:ANOTSS>2.0.CO;2).
- Vissa, N. K., Satyanarayana, A. N. V., & Kumar, B. P. (2013). Response of upper ocean and impact of barrier layer on Sidr cyclone induced sea surface cooling. *Ocean Science Journal*, *48*(3), 279–288.
- Wada, A. (2015). Verification of tropical cyclone heat potential for tropical cyclone intensity forecasting in the Western North Pacific. *Journal of Oceanography*, *71*(4), 373–387. <https://doi.org/10.1007/s10872-015-0298-0>.
- Walker, N. D., Leben, R. R., & Balasubramanian, S. (2005). Hurricane-forced upwelling and chlorophyll a enhancement within cold-core cyclones in the Gulf of Mexico. *Geophysical Research Letters*, *32*, 1–5. <https://doi.org/10.1029/2005GL023716>.
- Wang, J. W., & Han, W. (2014). The Bay of Bengal upper-ocean response to tropical cyclone forcing during 1999. *Journal of Geophysical Research, Oceans*, *119*, 98–120. <https://doi.org/10.1002/2013JC008965>.
- Yablonsky, R., & Ginis, I. (2009). Limitation of one-dimensional ocean models for coupled hurricane–ocean model forecasts. *Monthly Weather Review*, *137*, 4410–4419. <https://doi.org/10.1175/2009MWR2863.1>.
- Zheng, Z. W., Ho, C. R., & Kuo, N. J. (2008). Importance of pre-existing oceanic conditions to upper ocean response induced by super typhoon Hai-Tang. *Geophysical Research Letters*, *35*, 1–5. <https://doi.org/10.1029/2008GL035524>.
- Zheng, Z. W., Ho, C. R., Zheng, Q., Lo, Y. T., Kuo, N. J., & Gopalakrishnan, G. (2010). Effects of preexisting cyclonic eddies on upper ocean responses to Category 5 typhoons in the western North Pacific. *Journal of Geophysical Research, Oceans*, *115*, 1–11. <https://doi.org/10.1029/2009JC005562>.

Publisher's note Springer Nature remains neutral with regard to jurisdictional claims in published maps and institutional affiliations.